

# Thermodynamics and Kinetics of Sulfur Cathode during Discharge in MgTFSI<sub>2</sub>–DME Electrolyte

Tao Gao, Xiao Ji, Singyuk Hou, Xiulin Fan, Xiaogang Li, Chongying Yang, Fudong Han, Fei Wang, Jianjun Jiang, Kang Xu, and Chunsheng Wang\*

Rechargeable magnesium/sulfur battery is of significant interest because its energy density (1700 Wh kg<sup>-1</sup> and 3200 Wh L<sup>-1</sup>) is among the highest of all battery chemistries (lower than Li/O<sub>2</sub> and Mg/O<sub>2</sub> but comparable to Li/S), and Mg metal allows reversible operation (100% Coulombic efficiency) with no dendrite formation. This great promise is already justified in some early reports. However, lack of mechanistic study of sulfur reaction in the Mg cation environment has severely hindered our understanding and prevents effective measures for performance improvement. In this work, the very first systematic fundamental study on Mg/S system is conducted by combining experimental methods with computational approach. The thermodynamics and reaction pathway of sulfur cathode in MgTFSI<sub>2</sub>–DME electrolyte, as well as the associated kinetics are thoroughly investigated. The results here reveal that sulfur undergoes a consecutive staging pathway in which the formation and chain-shortening of polysulfide occur at early stage accompanied by the dissolution of long-chain polysulfide, and solid-state transition from short-chain polysulfide to magnesium sulfide occurs at late stage. The former process is much faster than the latter due to the synergetic effect of the mediating effect of dissolved polysulfide and the fast diffusion of Mg ion in the amorphous intermediate.

Rechargeable magnesium battery is of particular interest among all beyond Li-ion batteries, because of the highly reversible and dendrite-free Mg anode,<sup>[1]</sup> its low reduction potential (–2.36 V vs standard hydrogen electrode (SHE)), and high capacity (2205 mA h g<sup>-1</sup> and 3833 mA h cc<sup>-1</sup>).<sup>[2]</sup> Intensive efforts have been made in cathode materials development,<sup>[3–7]</sup> and among them sulfur is very appealing due to the high energy

density of Mg/S chemistry (1700 Wh kg<sup>-1</sup> and 3200 Wh L<sup>-1</sup>). Motivated by such potential, several concept cells were reported.<sup>[8–12]</sup> These work, obtaining capacities of 800–1200 mA h g<sup>-1</sup> with major discharge plateaus at 1.1–1.7 V for tens of cycles, proved that a rechargeable Mg/S chemistry is feasible, but with many fundamental questions to be answered.

One issue is that the reported electrochemical performance (discharge/charge curve, voltage hysteresis, etc.) has many discrepancies, which result in confusion in understanding of this system. Regarding the discharge/charge curve, one discharge plateau followed by a long slope is observed in some studies,<sup>[9,10,13]</sup> while there was only one plateau,<sup>[8,11,14]</sup> or only a slope in others.<sup>[12]</sup> Regarding voltage hysteresis, small voltage hysteresis were observed in some studies,<sup>[9–12]</sup> but huge hysteresis were reported in others.<sup>[14–17,8]</sup> Equally interesting is the reaction kinetics: the discharge/charge of Mg batteries are usually accompanied by large overpotential due to the sluggish solid-state diffusion of Mg<sup>2+</sup>.<sup>[18,19,6]</sup> Surprisingly, the hysteresis of Mg/S and Mg/Se chemistries can be remarkably small.<sup>[10,11,20]</sup> Although the solid–liquid two-phase reaction was cited as a probable cause for the fast kinetics observed therein, it remains unclear if any other factors exist and which is rate limiting. Understanding these fundamental questions is crucial to address the critical issues blocking the conversion of this promising chemistry into usable technology.

In this work, we aim to fill this knowledge gap. By combining experimental and computational approaches, we thoroughly examined the thermodynamics and reaction pathways of sulfur cathode in Mg battery chemistry and investigated the key kinetic limitations of the electrochemical reaction. Based on the proposed reaction mechanism and the associated thermodynamic and kinetics analysis, we are able to conclude a comprehensive view on the electrochemical performance of sulfur cathode in Mg chemistry. This understanding will help to explain these discrepancies and significantly benefit the future Mg/S battery study.

Electrolytes that can be used for Mg/S battery are listed in our previous work.<sup>[21]</sup> Since bis(trifluoromethane)sulfonimide (TFSI)–glyme is currently the standard electrolytes for studying sulfur chemistry for battery applications,<sup>[22–24]</sup> it would be a good

Dr. T. Gao, X. Ji, S. Hou, Dr. X. Fan, X. Li, Dr. C. Yang, F. Han, Dr. F. Wang, Prof. C. Wang  
Chemical and Biomolecular Engineering  
University of Maryland  
College Park, MD 20740, USA  
E-mail: cswang@umd.edu

Prof. J. Jiang  
School of Optical and Electronic Information  
Huazhong University of Science and Technology  
Wuhan, Hubei 430074, China

Dr. K. Xu  
Electrochemistry Branch  
Power and Energy Division Sensor and Electron Devices Directorate  
U.S. Army Research Laboratory  
Adelphi, MD 20783, USA

DOI: 10.1002/adma.201704313

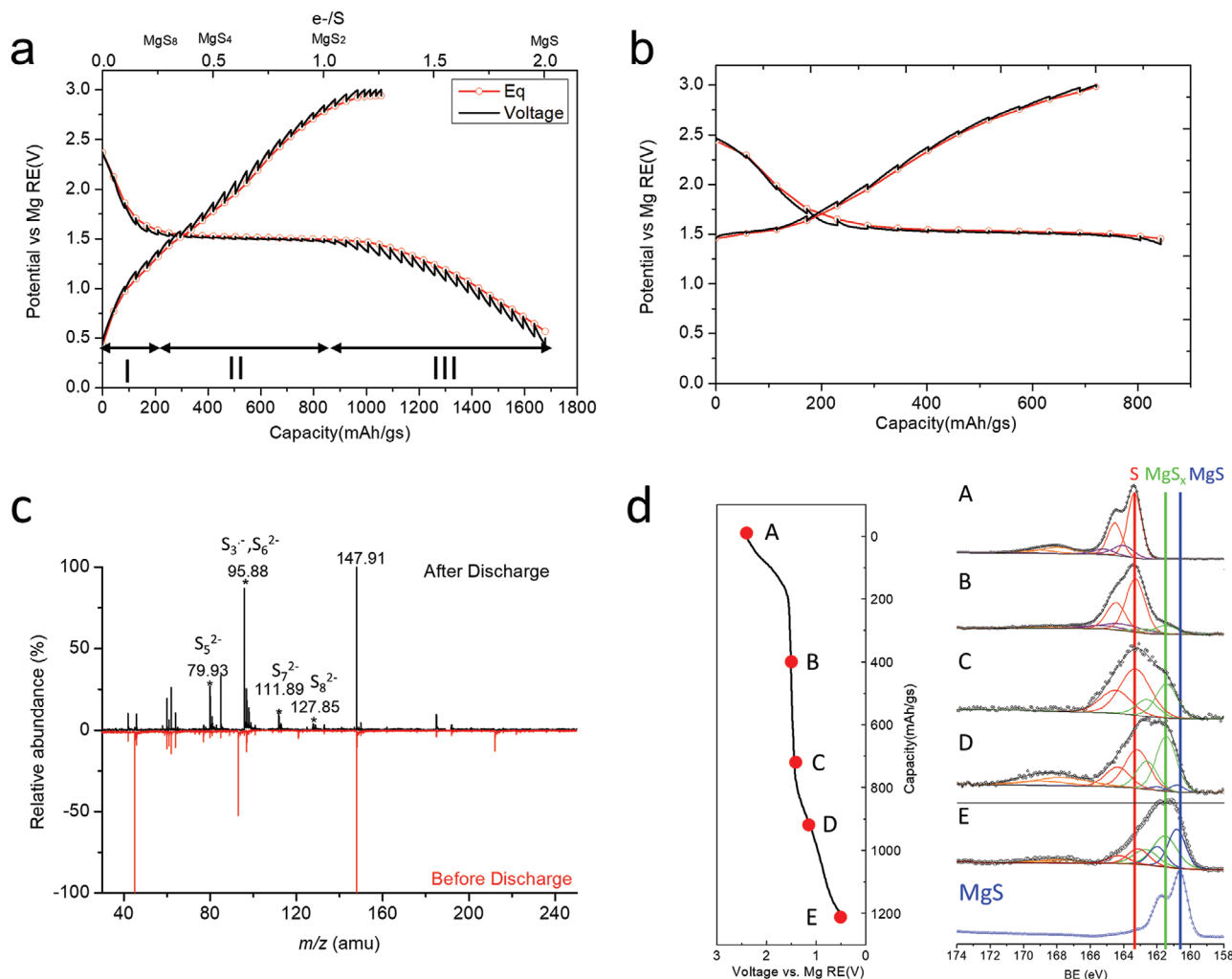


**Figure 1.** a,b) Thermodynamic equilibrium potential. Current: 50 mA g<sup>-1</sup>. Discharge time: 1 h, Rest time: 4 h; sulfur/carbon (S/C) ratio = 0.11. Red: equilibrium curve; black: transient potential; blue: current. c) ESI-MS spectra of electrolytes before and after discharge; d) High-resolution XPS S 2p spectra of sulfur cathode at different discharge states.

start to compare the electrochemical behavior of sulfur cathode in Mg cation environment and Li cation environment using the similar TFSI–glyme system. In this work, we use 0.5 M MgTFSI<sub>2</sub>–1,2-dimethoxyethane (DME) as the electrolyte. The cyclic voltammogram (Figure S1, Supporting Information) as well as the morphology of cycled Mg electrodes in this electrolyte (Figure S2, Supporting Information) both demonstrate its capability for reversible Mg deposition/stripping, consistent with previous studies.<sup>[25,26]</sup> Since large overpotential is needed for Mg deposition/stripping in this electrolyte,<sup>[26,27]</sup> we use three-electrode cell with Mg metals as both counter and reference electrodes, instead of two-electrode cell, to record the potential of sulfur cathode, so that the polarization of Mg counter electrode can be excluded. The thermodynamics of sulfur cathode at different magnesia-tion degree was investigated with galvanostatic intermittent titration technique (GITT). Similar to Li/S system,<sup>[28]</sup> the equilibrium potential of sulfur (red, Figure 1a,b) reveals clear staging features with several distinct processes occurring successively upon reduction: the initial slope (2.4–1.5 V), a plateau (1.5 V) and another

slope (1.5–0.5 V). The cumulative discharge capacity is close to the theoretical value, also achievable by galvanostatic discharge (Figure S3, Supporting Information), indicating the full utilization of sulfur at quasi-equilibrium condition in the sulfur/carbon composite electrode. These results suggest that kinetic limitation is a main obstacle to fully access the capacity of sulfur in previous studies.<sup>[9–11]</sup> In contrast to the discharge, complete recharge is not possible even under the same equilibrium condition, implying the formed (poly)sulfide is electrochemically difficult to be oxidized.<sup>[20]</sup> A similar equilibrium curve only discharged to 1.4V (Figure 1b) shows much higher reversibility, i.e., ~86% compared with that of ~60% when the cell is discharged to 0.5 V, indicating the reaction reversibility is highly dependent on the final discharge product.

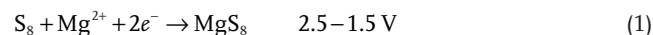
The electron transferred per S atom and the corresponding polysulfide intermediates (the upper  $x$ -axis in Figure 1a) are labeled. The three consecutive regions correspond to (I) S<sub>8</sub> → MgS<sub>8</sub>, (II) MgS<sub>8</sub> → MgS<sub>2</sub>, and (III) MgS<sub>2</sub> → MgS transformations, respectively. Interestingly, Li/S chemistry shows similar staging phenomena in ether-based electrolytes: (I) S<sub>8</sub> → Li<sub>2</sub>S<sub>8</sub>

(a short plateau between 2.2 and 2.3 V), (II)  $\text{Li}_2\text{S}_8 \rightarrow \text{Li}_2\text{S}_4$  (a slope between 2.3 and 2.0 V), (III)  $\text{Li}_2\text{S}_4 \rightarrow \text{Li}_2\text{S}_2 + \text{Li}_2\text{S}$  (a long plateau at 2.0 V), and (IV)  $\text{Li}_2\text{S}_2 \rightarrow \text{Li}_2\text{S}$  (a slope between 2.0 and 1.5 V).<sup>[28]</sup> To examine if there is any polysulfides dissolved during battery discharge, electrospray-ionization mass spectrometry (ESI-MS) was used to monitor the change of electrolyte composition (Figure 1c). The detected species are summarized in Table S1 in the Supporting Information. Apparently, only long-chained polysulfide ( $\text{S}_x^{2-}$ ,  $x = 8, 7, 6, 5$ ) and  $\text{S}_3^-$  radical are soluble, while short-chained polysulfide ( $\text{S}_x^{2-}$ ,  $x = 3, 2$ ) are entirely absent in the solution. The presence of  $\text{S}_4^{2-}$  cannot be determined since its position overlaps with the signals from the electrolyte ( $m/z = 63.93$ ). Hence, it can be concluded that the discharge is accompanied by the dissolution of long-chained polysulfide, which include  $\text{S}_x^{2-}$ , ( $x = 8, 7, 6, 5$ ) and possibly  $\text{S}_4^{2-}$ . The solubility of polysulfide (in the unit of atomic sulfur) is measured to be  $<50 \times 10^{-3} \text{ M}$ , which is lower than the solubility of  $\text{Li}_2\text{S}_8$  ( $6046 \times 10^{-3} \text{ M}$ ) by at least two orders of magnitude in the same TFSI-glyme system.<sup>[29]</sup>

Despite polysulfide dissolution, it is surprising that, under such equilibrium conditions, the effect of polysulfide shuttling is absent as it is usually observed for Li/S chemistry in ether-electrolytes.<sup>[30]</sup> A possible rationale for this phenomenon could be the low solubility of Mg polysulfide so that the shuttle effect (a form of self-discharge during charging) is negligible. This scenario has been seen in Li/S battery using concentrated electrolyte<sup>[31]</sup> or nonsolvent electrolyte<sup>[30]</sup> where polysulfide shuttle is suppressed due to the low solubility of polysulfide. Meanwhile, since shuttling is intrinsic chemical discharge inside the battery, its rate is dependent on how fast metal anode can reduce the polysulfide species. Given the much less reductive nature of Mg compared with Li, it is reasonable to assume that polysulfide reduction on Mg surface occurs at much slower rate than that on Li surface.

Based on these observations, we propose the following reaction pathway during sulfur reduction.

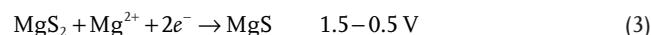
*Stage I:* Sulfur is partially reduced and forms a long-chain polysulfide. The sloping potential also indicates that polysulfide solubility does not increase remarkably, otherwise a short plateau for the solid-liquid two-phase reaction would appear, similar to the  $\text{S}_8$ - $\text{Li}_2\text{S}_8$  plateau in Li/S battery



*Stage II:* The reaction is accompanied by the shortening of polysulfide chain. Considering the polysulfide solubility is small, sulfur species mainly exist in the solid state. The phase transition from long-chain polysulfide to  $\text{MgS}_2$  (Equation (2)) may explain the potential plateau. Despite no Mg/S binary compounds with high sulfur content ( $\text{MgS}_x$ ,  $x = 2-8$ ) are found experimentally,<sup>[32]</sup>  $\text{MgS}_2$  with modified rock salt structure is predicted by ab initio calculation while other polysulfides seem only exist in amorphous state.<sup>[33]</sup> The liquid (long-chain polysulfide) to solid ( $\text{MgS}_2$ ) phase transition may also explain the potential plateau



*Stage III:* Since no  $\text{S}_2^{2-}$  or  $\text{S}^{2-}$  can be found in the electrolyte, the entire reaction occurs in the solid state. Similar to the Stage IV in Li/S system,<sup>[28]</sup> this step proceeds with very slow kinetics. Large overpotential was clearly observed in the Coulombic titration experiment (Figure S4, Supporting Information). For Stages I and II, the potentials are close to equilibrium after rest. In Stage III, however, the potentials are still under dynamic change even after 4 h rest. Since the potential observed in this stage is off equilibrium, the absence of a potential plateau for phase change is understandable. For the convenience of discussion, we will still use equilibrium potential to denote the observed potential in this stage during the GITT experiment



To verify the mechanism, x-Ray photoelectron spectroscopy (XPS) S 2p spectra of sulfur cathodes at different discharge states are collected (Figure 1d). The pristine carbon/sulfur composite (position A) shows two S 2p<sub>3/2</sub> peaks located at 163.3 eV (red) and 164.1 eV (purple) corresponding to S, in agreement with previous study using the same microporous carbon/sulfur composite cathode.<sup>[34]</sup> Upon discharge to B, a new S 2p<sub>3/2</sub> peak at  $\approx 161.5 \text{ eV}$  (green) appears between MgS (160.6 eV) and S (163.3 eV), indicating the formation of Mg polysulfide  $\text{MgS}_x$  ( $x = 2-8$ ). Further, discharge to C strengthens this peak and continuously weakens S. Another new peak emerges at D, corresponding to the formation of final product MgS. Continuous discharge leads to further growth of MgS peak at the expense of both S and  $\text{MgS}_x$ . Thus, XPS result confirms the transient formation of Mg polysulfide  $\text{MgS}_x$  ( $x = 2-8$ ) as the intermediate product and MgS as the final product. The fact that MgS peak (blue) does not appear until D agrees with the proposed mechanism that sulfur reduction occurs in consecutive steps. The continuous growth of MgS peak and weakening of  $\text{MgS}_x$  peak after position D reaffirms that Stage III involves phase transition from  $\text{MgS}_x$  to MgS. The fact that elemental sulfur peak does not disappear during discharge was also observed in studies using similar carbon/sulfur composites cathode.<sup>[35,36]</sup> We speculate this could be due to the presence of some elemental sulfur far from the reaction frontier (the electrode/electrolyte interface). This is possible if the rate of phase transformation ( $\text{S} \rightarrow \text{MgS}_x \rightarrow \text{MgS}$ ) and  $\text{Mg}^{2+}$  diffusion fail to keep pace with the rate of magnesiation. As a consequence, a nonuniform distribution of reaction products perpendicular to the reaction frontier can be expected with Mg rich phase residing on top of Mg poor phase. Nevertheless, a continuous declining intensity of S 2p<sub>3/2</sub> peak located at 163.3 eV suggests the consumption of elemental sulfur during battery discharge.

We further conduct ab initio molecular dynamics (AIMD) simulation to investigate polysulfide structure (Figure S5a, Supporting Information). All polysulfides  $\text{MgS}_x$  ( $x = 2-8$ ) are amorphous, while an ordered structure emerges once the composition reaches MgS, agreeing with the fact that MgS is the only found crystalline Mg-S binary compound in inorganic crystal structure database (ICSD) database.<sup>[32]</sup> The partial pair distribution functions (PDFs) are calculated to characterize the quantity of Mg-S and S-S bond. The distance of Mg-S and S-S pairs of  $\text{MgS}_8$  and MgS (Figure S5b, Supporting Information) is in good agreement with the experimental value (Figure S5c,

Supporting Information). Starting from  $\text{MgS}_8$ , increasing Mg concentration breaks S–S bonds (weakening of peak black i) while creating Mg–S bond (sharpening of peak red i). When the composition reaches  $\text{MgS}$ , all S–S bonds at 2.0 Å are gone. This process is summarized schematically in Figure S5d in the Supporting Information. Clearly, with increasing Mg concentration, the numbers of Mg–S bond grows while the number of S–S bond declines. These results well suggest that during the discharge polysulfide,  $\text{MgS}_x$  is experiencing a continuous chain-shortening and eventually turns into  $\text{MgS}$ .

Due to its insulating nature, sulfur is usually mixed with carbon to enhance its accessibility to electrons. In the above thermodynamics analysis, sufficient carbon ( $\text{S/C} = 0.11$ ) ensures full sulfur utilization and thus a comprehensive view of the Mg–S phase diagram. The overpotentials of the electrochemical reaction (Figure 2a) are obtained by comparing the equilibrium potential (red, Figure 1a) with the transient potential (black, Figure 1a). Clearly, it consists of three distinct stages, consistent with the three-stage potential profile (Figure 1a). Overall, the reaction kinetics is much more facile in Stages I and II than in Stage III.

Cyclic voltammetry tests were carried out (Figure 2b) and three cathodic peaks (a, b, and c) corresponding to Stages I, II, and III can be observed. Zoom-in of the CV results is provided in Figure S6 in the Supporting Information for better illustrating the three reduction peaks. The current densities of the reduction peaks a, b, and c are plotted with log axis (Figure 2c),

and linear trends can be observed for all three peaks. The kinetic factor that dominates the reduction reaction can be identified on the basis of  $b$  value by fitting the data to equation  $i = av^b$ , where  $b = 1$  represents a surface-controlled reaction and  $b = 0.5$  represents a diffusion-controlled reaction.<sup>[37]</sup> The  $b$  values for Stages I and II are 0.73 and 0.63, respectively, indicating a mix-controlled reaction: the presence of soluble long-chain polysulfide triggers a surface reaction in parallel to the solid-state reduction of sulfur. The  $b$  value for Stage III is 0.53, indicating a diffusion-controlled reaction, which arises from the solid-state reaction nature of this stage: there is an Mg concentration gradient across the active material, and the reduction of  $\text{MgS}_x$  and S deep from interface is limited by the diffusion of  $\text{Mg}^{2+}$ . The diffusivity of  $\text{Mg}^{2+}$  at 600 K was calculated with AIMD simulations (Figure 2d). The highest diffusivity is seen when magnesiation just starts, then it declines monotonically as more  $\text{Mg}^{2+}$  is inserted, but the decrease is within one order of magnitude before  $\text{MgS}_2$ . However, a drop of three orders of magnitude is seen when the composition reaches  $\text{MgS}$ . This extremely low diffusivity is not surprising since  $\text{MgS}$  shows strong tendency to crystallize, while  $\text{MgS}_x$  ( $x = 2\text{--}8$ ) tends to maintain an amorphous structure. It partially explains the rapid rise of overpotential when the reaction enters into Stage III: once  $\text{MgS}$  is formed at the interface,  $\text{Mg}^{2+}$  diffusion becomes extremely difficult.

To investigate the effect of carbon amount on the kinetics, GITT curves at different S/C ratios are obtained (Figure 2e).

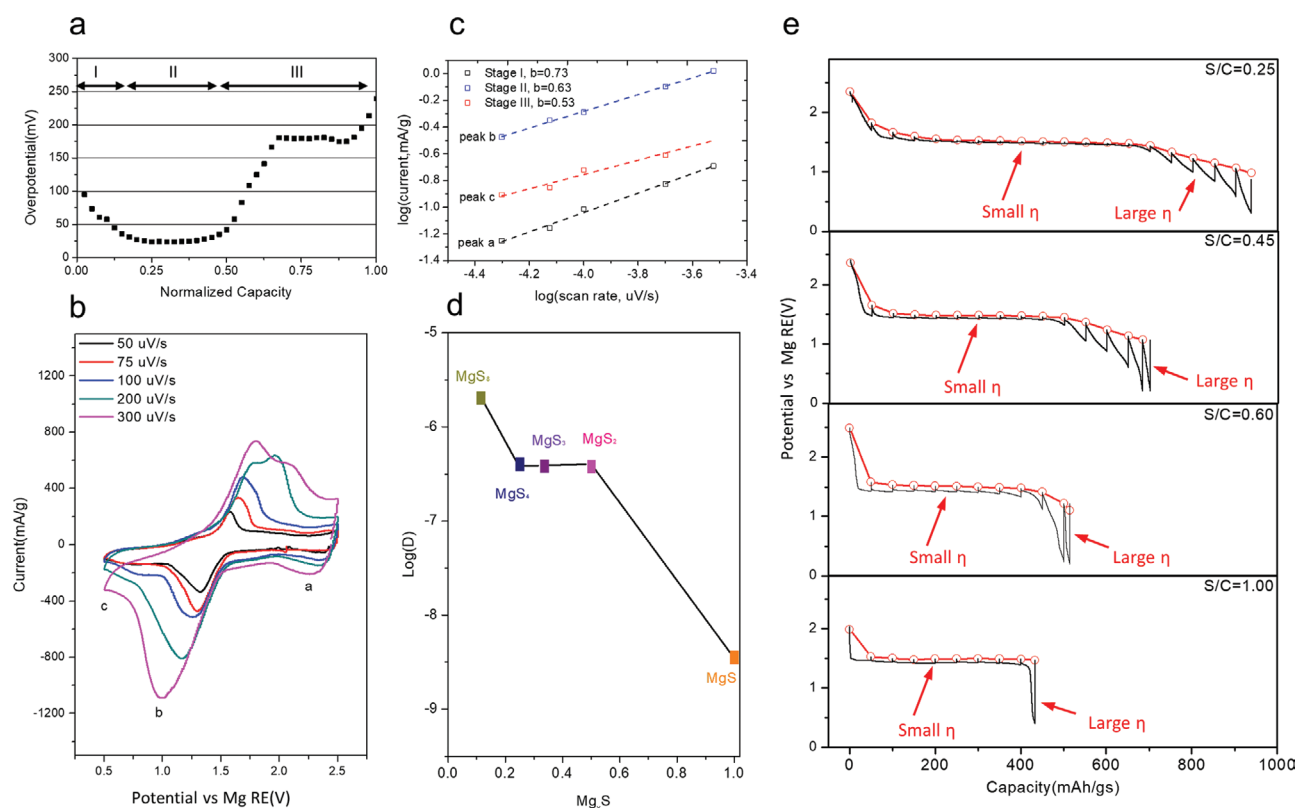


**Figure 2.** a) Overpotential of GITT discharge; b) cyclic voltammetry curves at different scan rates. Zoom-in of the CV curves is given in Figure S6 in the Supporting Information; c) kinetic fitting of the peak current by equation  $i = av^b$ ,  $i$  is the peak current density, and  $v$  is the scan rate; d) calculated diffusivities of  $\text{Mg}^{2+}$  in  $\text{MgS}_x$ ,  $x = 2\text{--}8$  and  $\text{MgS}$  at 600 K. e) GITT curves of sulfur cathode with different S/C ratios.

The three-stage reaction pattern is maintained in all curves; however, the overall capacity decreases severely with increasing S/C ratio. The small overpotentials in Stages I and II suggest that the kinetics are insensitive to S/C ratio in these two stages, i.e., the transport of electrons to the reaction sites is not rate limiting. This is likely due to (1) the soluble long-chain polysulfide, once formed, can easily diffuse to sites where electrons are more readily available, and (2) it can function as a redox mediator, which passes electrons to other reaction sites. Such redox mediating effect of polysulfide is well known in sulfur batteries.<sup>[38–40]</sup> However, the large solubility difference of polysulfide (two orders of magnitude) in Li/S and Mg/S has resulted in the decreasing capacity in Stages I/II at high S/C ratio: in Li/S, sufficient dissolution of the formed intermediate polysulfides enables continuous exposure of sulfur underneath the reaction site, while in Mg/S, the partial dissolution of polysulfides renders most polysulfide to remain in the solid state. Magnesiumation of sulfur species in the bulk relies on the solid state diffusion of  $Mg^{2+}$ . Once all the dissolved polysulfides are consumed, reaction enters Stage III, and the large overpotential of the solid-state reaction leads to early termination of discharge. Because sulfur species in the bulk are still not fully reduced, a low capacity (average utilization of sulfur) is observed, especially at high S/C ratio (thicker sulfur species layer).

The galvanostatic discharge/charge curves bear the signature three-stage pattern (Figure 3), but the obtainable capacity is lower than the theoretical value due to kinetic limitation. Stages I and II together contribute  $\approx 800 \text{ mA h g}^{-1}$ , while Stage III only contributes  $\approx 400 \text{ mA h g}^{-1}$  due to its especially inferior kinetics. Discharge/charge in 1.4–3.0 V (Figure 3b) show a much higher initial Coulombic efficiency, consistent with the thermodynamics analysis. Remarkably, Stage II shows negligible hysteresis ( $<0.1 \text{ V}$ ). A typical potential profile with high S/C ratio (Figure S7, Supporting Information) shows that the discharge terminates as soon as reaction enters Stage III. Coulombic efficiency gradually increases in the initial cycles to

$\approx 100\%$  (Figure 3c), but it is close to 100% in the first cycle if the cell is only discharged to 1.4 V (Figure 3d). This difference demonstrates that the reversibility of Mg/S chemistry is highly dependent on discharge product: S/ $MgS_x$  is  $\approx 100\%$  reversible but S/MgS is only 82% reversible. In general, several reasons may account for the capacity loss during cycling: (1) loss of active material due to the dissolution of S and  $MgS_x$  (despite their low solubility); (2) volume expansion during magnesiumation and the associated fracture of the composite electrode, which renders some active material to lose contact with carbon matrix. Although in Mg/S cells, the volume of the active material only expands by 22% even after fully discharge, in sharp comparison with  $\approx 80\%$  in Li/S cells, the solid-state reaction route could further exaggerate the degradation from mechanical strain; (3) difficulty in reoxidization of the formed MgS (less electrochemical activity of more magnesiumated sulfur). This is evidenced by the decreased reversibility of MgS compared with  $MgS_x$ . As far as we know, only the first cause has been well accepted, but few attentions are paid to the other two causes. Particularly, it is for the first time that the third cause, discharge-depth depend reversibility, is proposed as a cause for the capacity fading. Indeed, the cycling stability can be dramatically improved if the main discharge product is controlled to be  $MgS_x$  with the dissolution of polysulfide suppressed, as demonstrated in our recent work.<sup>[21]</sup>

Overall, the reaction pathway is schematically summarized in Figure 4. Sulfur is impregnated onto the wall of porous carbon and the vacant space in the pores is filled with electrolyte (Figure 4a). All the kinetic processes are illustrated with different colors (Figure 4b) and are labeled in the sulfur reduction pathway (Figure 4d). Before discharge, a small amount of sulfur dissolves and the rest resides on the wall of pores. In Stage I, magnesiumation of sulfur leads to formation of  $MgS_8$ . In Stage II, magnesiumation leads to gradual chain-shortening of polysulfide ( $MgS_8 \rightarrow MgS_7 \rightarrow MgS_6 \rightarrow MgS_5 \rightarrow MgS_4 \rightarrow MgS_2$ ), in which  $MgS_x$  ( $x = 4–8$ ) is soluble but  $MgS_2$  is insoluble. Since

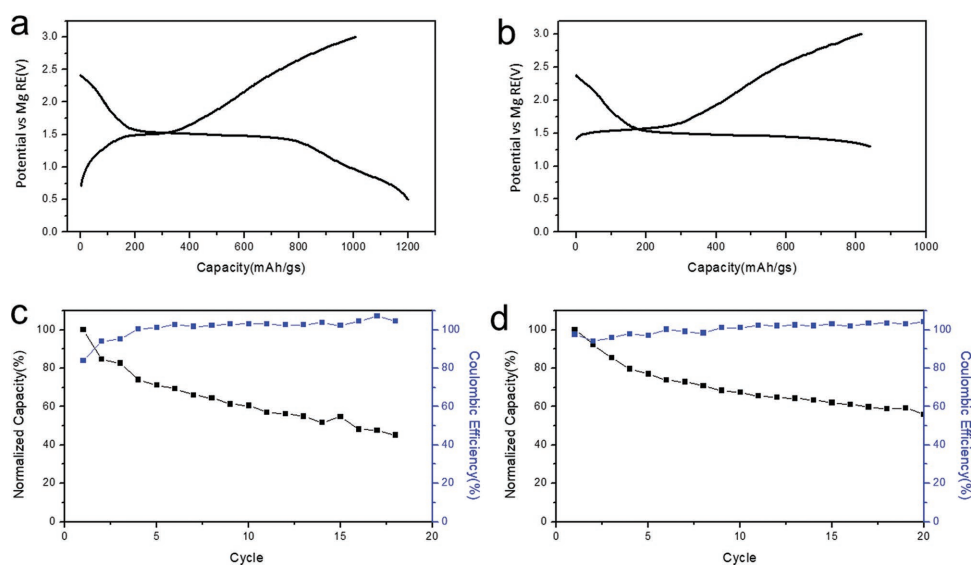


**Figure 3.** Electrochemical Performance. a,b) First cycle discharge/charge curves; c,d) cycling performance and Coulombic efficiency, current:  $100 \text{ mA g}^{-1}$ .

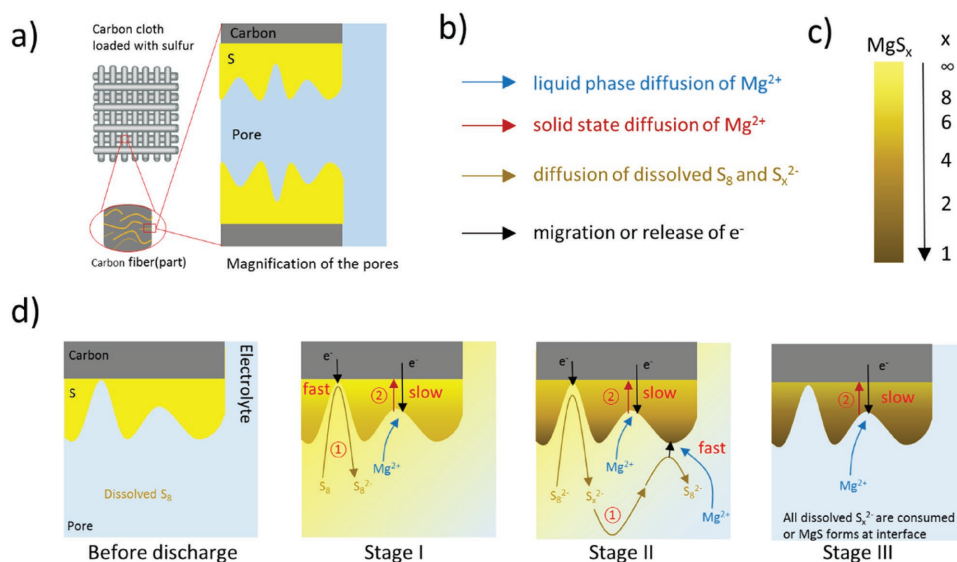


**Figure 4.** Schematic of sulfur reduction mechanism. a) The structure of the carbon/sulfur composite cathode. The carbon wall is covered by a sulfur layer with nonuniform thickness. b) The kinetic processes during discharge. c) Concentration of Mg in Mg-S binary compound. d) Sulfur reduction mechanism. ① Surface magniesiation. ② Bulk magniesiation. Stages I/II involve both surface magniesiation and bulk magniesiation so their kinetics are mixed-controlled, and Stage III has only bulk magniesiation so its kinetics is diffusion controlled.

the solubility of long-chain polysulfide  $\text{MgS}_x$  ( $x = 8-4$ ) is only tens of  $\times 10^{-3}$  M, most sulfur species should exist in the solid phase so that an Mg concentration gradient in the solid phase is expected (Figure 4c is the concentration map). For the dissolved long-chain polysulfide, they can easily diffuse in the electrolyte to sites where electrons are more available and be partially reduced, and then pass the electrons to other reaction sites to reduce the undissolved surface  $\text{MgS}_x$  through disproportionation reaction. For this reason, magniesiation of surface  $\text{MgS}_x$  is fast due to its easy access of  $\text{Mg}^{2+}$  and  $e^-$  (carried by dissolved polysulfide); however, magniesiation of bulk  $\text{MgS}_x$  is limited by the sluggish diffusion of  $\text{Mg}^{2+}$  and solid-state transport of  $e^-$ . Once all the soluble long-chain polysulfide  $\text{MgS}_x$  ( $x = 8-4$ ) are reduced to insoluble  $\text{MgS}_2$ , reaction enters Stage III, in which magniesiation only proceeds through solid state. The large overpotential associated with the slow kinetics will cause sharp potential drop, resulting in the early termination of discharge. As a result of this kinetic limitation, sulfur utilization decreases with increasing S/C ratio when sulfur layer thickness is increased so that bulk reaction dominates and less “naked carbon” (uncovered carbon surface and/or carbon surface covered by a very thin sulfide layer ( $<$ tunnel thickness)) is present to provide easy electrons. Notably, the GITT curve of Li/S system in LiTFSI-DEMETFSI ionic liquid electrolyte also shows similar three-stage pattern:<sup>[41]</sup> Stages I and II show fast kinetics and contribute to half of the theoretical capacity, while Stage III shows sluggish kinetics. This is in excellent consistency with what was observed in the work, revealing the similarity in sulfur reduction pathway where the dissolution of polysulfide is greatly inhibited.<sup>[41]</sup>

In summary, sulfur reduction occurs through two parallel but interacting pathways in Mg batteries: (1) surface magniesiation where the dissolved polysulfide passes  $e^-$  to reaction site as a redox mediator and  $\text{Mg}^{2+}$  is readily obtained from the

electrolyte; and (2) bulk magniesiation which requires solid-state transport of  $\text{Mg}^{2+}$  and  $e^-$ . Note the definition of the two reaction pathways only specifies where magniesiation takes place. Stages I/II involve both reaction pathways so their kinetics are mixed-controlled. Once all the dissolved polysulfides are consumed so that no more easy  $e^-$  from polysulfide, or maximum magniesiation is achieved at the interface ( $\text{MgS}$ ), the discharge enters Stage III where magniesiation only occurs through the second pathway, and the kinetics becomes diffusion-controlled. At low S/C ratio, the first pathway dominates so high sulfur utilization can be realized, while low utilization is observed at high S/C ratio.

Based on the proposed reaction mechanism and the associated kinetics analysis, as well as the equilibrium potential of sulfur recorded in the three-electrode setup, we can conclude a comprehensive view on the electrochemical performance of sulfur cathode in Mg chemistry. This understanding will help to explain the discrepancies mentioned in the introduction. In general, the discharge curve shows the short slope (above 1.5 V), long plateau ( $\approx 1.5$  V), and then long slope (below 1.5 V) feature, but kinetics limitation can alter the discharge curve to different representations due to different kinetics at different stages. Factors that can affect kinetics include: current, sulfur loading (S/C ratio), and electrolyte chemistry. Voltage hysteresis of two-electrode cells is the combinational effect of cathode (sulfur) polarization and anode (Mg metal) polarization. Detail discussion is given below.

The influence of the kinetics is well manifested in the difference between the discharge curves under equilibrium (Figure 1a,b) and nonequilibrium (Figure 3a,b) conditions, and is exaggerated at high S/C ratio (Figure 2e; Figure S7, Supporting Information). Under an ideal condition (quasi-equilibrium where kinetic limitation is negligible, e.g. S/C = 0.11 and GITT discharge), when all sulfur is utilized the discharge curve is featured by three stages: a short slope ( $\text{S}_8$ - $\text{MgS}_8$ ), a long plateau

(MgS<sub>8</sub>–MgS<sub>2</sub>) followed by a long slope (MgS<sub>2</sub>–MgS) (Figure 1a,b), but when a finite current is applied ( $S/C = 0.11$ ,  $100 \text{ mA g}^{-1}$ ) all three stages are shortened especially the third one due to its sluggish kinetics (Figure 3a,b). Such discharge voltage profiles are most commonly observed in previous studies,<sup>[9,10,13,16]</sup> and in our experiments with different sulfur/carbon composite cathodes (Figures S8 and S9, Supporting Information). When sulfur loading is gradually increased (increasing  $S/C$  from 0.11 to 1.0), Stages I/II are getting shorter because bulk magnesiation becomes more dominating, and Stage III is also getting shorter in a much severer manner due to the worsening reaction kinetics resulting from the increasing diffusion length (Figure 2e). In the extreme case, the discharge curve shows only one plateau, as observed in our experiment (Figures S7 and S10, Supporting Information) and previous studies.<sup>[11,14]</sup> (Note two-electrode cells were used in these studies so the overpotential of Mg anode is included in the reported voltage). Other than sulfur loading and current, the chemistry of electrolyte also plays a crucial role on determining the discharge curve, because the first reaction pathway relies on the dissolution of polysulfide. When the dissolution of polysulfide is enhanced in certain electrolytes, the discharge plateau will be tilted so that the boundary between Stages I, II, and III will become blurred, as observed in our experiment (Figures S11 and S12, Supporting Information) and previous studies.<sup>[23]</sup> In our experiment, we also found that the choice of carbon host can have a significant influence on the kinetics even at similar sulfur loading (Figures S8–S10, Supporting Information; Figure 2e), which is worthy of further investigation. As for the large voltage hysteresis observed in some studies, our thermodynamic analysis reveals that the voltage hysteresis of the discharge/charge profile (Figure 3a) is quite small ( $<0.2 \text{ V}$  for the plateau). Due to the usage of a three-electrode setup, this hysteresis reflects true polarization of sulfur cathode during reaction, but exclude any contribution from Mg anode. Since most of the reported Mg/S studies were performed in two-electrode cells,<sup>[14–17,8]</sup> it is highly possible that the anode overpotential is the main cause for the large voltage hysteresis. Our recent study proved this speculation, as the Mg anode overpotential (0.45) contributes to 60% of the total voltage hysteresis in a Mg/S battery with MgTFSI<sub>2</sub>–MgCl<sub>2</sub>–DME electrolyte.<sup>[21]</sup>

To address this kinetic limitation at high  $S/C$  ratio (which is more relevant for practical Mg/S battery), future efforts should focus on improve the kinetics of bulk magnesiation and/or enhance the surface magnesiation. The former can be achieved by mixing the insulating sulfur with more conducting transition metal sulfide<sup>[4,42]</sup> to form a better electronic/ionic conducting network, using different carbon host (Figures S8–S10, Supporting Information), or adding Lewis acid mediator to activate the formed magnesium sulfide,<sup>[10]</sup> and the latter can be realized by tuning the chemistry of the electrolyte to obtain high polysulfide solubility (Figures S11 and S12, Supporting Information).

In conclusion, the thermodynamics, reaction pathway, and kinetics of sulfur cathode in Mg battery during discharge in MgTFSI<sub>2</sub>–DME electrolyte is thoroughly investigated for the first time in this work. We demonstrate that sulfur reduction occurs through three consecutive steps: Stage (I) elemental sulfur to long-chain polysulfide (potential slope in 2.4–1.5 V), Stage (II) chain-shortening of polysulfide (potential plateau at 1.5 V), and

Stage (III) solid-state transition from short-chain polysulfide to MgS (potential slope in 1.5–0.5 V). The reaction in Stage II shows the fastest kinetics with small overpotential ( $<0.1 \text{ V}$  at  $100 \text{ mA g}^{-1}$ ) due to the synergetic effect of a fast surface reaction enabled by the dissolved polysulfide and the relatively fast Mg<sup>2+</sup> diffusion in the amorphous MgS<sub>x</sub>, but the Stage III is very sluggish. Electrochemical cycling shows the reversibility of Mg/S chemistry significantly relies on the discharge product. Since its low solubility cannot ensure all formed polysulfide to be dissolved, formation of insoluble MgS<sub>x</sub> and MgS at the interface exerts a large barrier for further magnesiation, which leads to early termination of discharge and low sulfur utilization especially at high sulfur/carbon ratio.

This work provides the first in-depth understanding of sulfur chemistry for Mg battery application. TFSI–glyme electrolyte serves as a good benchmark electrolyte for carrying out the above investigations due to its simple chemical structure and wide usage in sulfur batteries. Nevertheless, the role of electrolyte should be given special attention in any future studies concerning the mechanism of Mg/S battery, because the chemical property of electrolyte can significantly affect the dissolution of Mg polysulfide, which in turn alters the sulfur reaction pathway. Similar to Li/S battery in ether–electrolytes, the electrochemical performance of the Mg/S battery in MgTFSI<sub>2</sub>–DME electrolyte also relies on the fast kinetics resulting from the dissolution of long-chain polysulfide. Nevertheless, the high sulfur loading cells show low sulfur utilization due to the low solubility of polysulfide, and persistent capacity fading caused by gradual loss of active materials, electrochemical inertness of MgS or mechanical fracture effect poses problem to the practical application of this promising cell chemistry. Future work will need to address these issues by removing these kinetic and mechanical barriers with the approaches mentioned in this work so that the potential benefits of Mg/S chemistry could be converted into practical technology.

## Experimental Section

The sulfur/carbon composite cathode was prepared with a melt-diffusion method by impregnating sulfur into the pores of active carbon cloth (ACC-507-20, Kynol Inc. USA) at  $155 \text{ }^\circ\text{C}$ . Sulfur loading was  $1 \text{ mg cm}^{-2}$  for  $S/C$  ratio = 0.11. In this study, MgTFSI<sub>2</sub>–DME was used as the electrolyte, since TFSI–glyme were currently the standard electrolytes for studying sulfur chemistry for battery applications. More experimental details can be found in the Supporting Information.

## Supporting Information

Supporting Information is available from the Wiley Online Library or from the author.

## Acknowledgements

T.G. and C.W. acknowledge the support from the Nanostructures for Electrical Energy Storage (NEES), an Energy Frontier Research Center funded by the US Department of Energy, Office of Science, Basic Energy Sciences, under Award number DESC0001160. T.G. also acknowledges the Dean's Dissertation Fellowship from University of Maryland.

## Conflict of Interest

The authors declare no conflict of interest.

## Keywords

kinetics, magnesium battery, reaction mechanism, sulfur, thermodynamics

Received: July 31, 2017

Revised: September 17, 2017

Published online:

- [1] J. Muldoon, C. B. Bucur, A. G. Oliver, T. Sugimoto, M. Matsui, H. S. Kim, G. D. Allred, J. Zajicek, Y. Kotani, *Energy Environ. Sci.* **2012**, *5*, 5941.
- [2] H. D. Yoo, I. Shterenberg, Y. Gofer, G. Gershinsky, N. Pour, D. Aurbach, *Energy Environ. Sci.* **2013**, *6*, 2265.
- [3] N. Sa, H. Wang, D. L. Proffit, A. L. Lipson, B. Key, M. Liu, Z. Feng, T. T. Fister, Y. Ren, C.-J. Sun, J. T. Vaughey, P. A. Fenter, K. A. Persson, A. K. Burrell, *J. Power Sources* **2016**, *323*, 44.
- [4] X. Sun, P. Bonnick, V. Duffort, M. Liu, Z. Rong, K. A. Persson, G. Ceder, L. F. Nazar, *Energy Environ. Sci.* **2016**, *9*, 2273.
- [5] R. Zhang, C. Ling, *ACS Appl. Mater. Interfaces* **2016**, *8*, 18018.
- [6] G. Vardar, E. G. Nelson, J. G. Smith, J. Naruse, H. Hiramatsu, B. M. Bartlett, A. E. S. Sleightholme, D. J. Siegel, C. W. Monroe, *Chem. Mater.* **2015**, *27*, 7564.
- [7] H. Tian, T. Gao, X. Li, X. Wang, C. Luo, X. Fan, C. Yang, L. Suo, Z. Ma, W. Han, C. Wang, *Nat. Commun.* **2017**, *8*, 14083.
- [8] H. S. Kim, T. S. Arthur, G. D. Allred, J. Zajicek, J. G. Newman, A. E. Rodnyansky, A. G. Oliver, W. C. Boggess, J. Muldoon, *Nat. Commun.* **2011**, *2*, 427.
- [9] Z. Zhao-Karger, X. Zhao, D. Wang, T. Diemant, R. J. Behm, M. Fichtner, *Adv. Energy Mater.* **2015**, *5*, 1401155.
- [10] T. Gao, M. Noked, A. J. Pearse, E. Gillette, X. Fan, Y. Zhu, C. Luo, L. Suo, M. A. Schroeder, K. Xu, S. B. Lee, G. W. Rubloff, C. Wang, *J. Am. Chem. Soc.* **2015**, *137*, 12388.
- [11] Z. Zhang, Z. Cui, L. Qiao, J. Guan, H. Xu, X. Wang, P. Hu, H. Du, S. Li, X. Zhou, S. Dong, Z. Liu, G. Cui, L. Chen, *Adv. Energy Mater.* **2017**, *7*, 1602055.
- [12] X. Yu, A. Manthiram, *ACS Energy Lett.* **2016**, *28*, 896.
- [13] Z. Zhao-Karger, M. E. Gil Bardaji, O. Fuhr, M. Fichtner, M. Fichtner, X. Wang, P. Hu, H. Du, S. Li, X. Zhou, S. Dong, Z. Liu, G. Cui, L. Chen, *J. Mater. Chem. A* **2017**, *5*, 10815.
- [14] W. Li, S. Cheng, J. Wang, Y. Qiu, Z. Zheng, H. Lin, S. Nanda, Q. Ma, Y. Xu, F. Ye, M. Liu, L. Zhou, Y. Zhang, *Angew. Chem., Int. Ed.* **2016**, *55*, 6406.
- [15] S. Y. Ha, Y. W. Lee, S. W. Woo, B. Koo, J. S. Kim, J. Cho, K. T. Lee, N. S. Choi, *ACS Appl. Mater. Interfaces* **2014**, *6*, 4063.
- [16] B. P. Vinayan, Z. Zhao-Karger, T. Diemant, V. S. K. Chakravadhanula, N. I. Schwarzburger, M. A. Cambaz, R. J. Behm, C. Kuebel, M. Fichtner, *Nanoscale* **2016**, *8*, 3296.
- [17] K. Itaoka, I.-T. Kim, K. Yamabuki, N. Yoshimoto, H. Tsutsumi, *J. Power Sources* **2015**, *297*, 323.
- [18] R. Zhang, X. Yu, K. W. Nam, C. Ling, T. S. Arthur, W. Song, A. M. Knapp, S. N. Ehrlich, X. Q. Yang, M. Matsui, *Electrochem. Commun.* **2012**, *23*, 110.
- [19] S. Rasul, S. Suzuki, S. Yamaguchi, M. Miyayama, *Solid State Ionics* **2012**, *225*, 542.
- [20] Z. Zhao-Karger, X.-M. Lin, C. Bonatto Minella, D. Wang, T. Diemant, R. J. Behm, M. Fichtner, *J. Power Sources* **2016**, *323*, 213.
- [21] T. Gao, S. Hou, F. Wang, Z. Ma, X. Li, K. Xu, C. Wang, *Angew. Chem., Int. Ed.* **2017**, <https://doi.org/10.1002/anie.201708241>.
- [22] X. Ji, K. T. Lee, L. F. Nazar, *Nat. Mater.* **2009**, *8*, 500.
- [23] S. Wenzel, H. Metelmann, C. Rieß, A. K. Dürr, J. Janek, P. Adelhelm, *J. Power Sources* **2013**, *243*, 758.
- [24] H. Ryu, T. Kim, K. Kim, J. H. Ahn, T. Nam, G. Wang, H. J. Ahn, *J. Power Sources* **2011**, *196*, 5186.
- [25] I. Shterenberg, M. Salama, H. D. Yoo, Y. Gofer, J.-B. Park, Y.-K. Sun, D. Aurbach, *J. Electrochem. Soc.* **2015**, *162*, A7118.
- [26] J. G. Connell, B. Genorio, P. P. Lopes, D. Strmcnik, V. R. Stamenkovic, N. M. Markovic, *Chem. Mater.* **2016**, *28*, 8268.
- [27] N. N. Rajput, X. Qu, N. Sa, A. K. Burrell, K. A. Persson, *J. Am. Chem. Soc.* **2015**, *137*, 3411.
- [28] S. S. Zhang, *J. Power Sources* **2013**, *231*, 153.
- [29] S. Zhang, K. Ueno, K. Dokko, M. Watanabe, *Adv. Energy Mater.* **2015**, 1500117.
- [30] M. Cuisinier, P.-E. Cabelguen, B. D. Adams, A. Garsuch, M. Balasubramanian, L. F. Nazar, *Energy Environ. Sci.* **2014**, *7*, 2697.
- [31] L. Suo, Y.-S. Hu, H. Li, M. Armand, L. Chen, *Nat. Commun.* **2013**, *4*, 1481.
- [32] M. Hellenbrandt, *Crystallogr. Rev.* **2004**, *10*, 17.
- [33] G. Mali, *Acta Crystallogr., Sect. C: Struct. Chem.* **2017**, *73*, 229.
- [34] T. Gao, X. Li, X. Wang, J. Hu, F. Han, X. Fan, L. Suo, A. J. Pearse, S. B. Lee, G. W. Rubloff, K. J. Gaskell, M. Noked, C. Wang, *Angew. Chem., Int. Ed.* **2016**, *55*, 9898.
- [35] M. Helen, M. A. Reddy, T. Diemant, U. Golla-Schindler, R. J. Behm, U. Kaiser, M. Fichtner, *Sci. Rep.* **2015**, *5*, 12146.
- [36] Y. Xu, Y. Wen, Y. Zhu, K. Gaskell, K. A. Cychosz, B. Eichhorn, K. Xu, C. Wang, *Adv. Funct. Mater.* **2015**, *25*, 4312.
- [37] H. Lindström, S. Södergren, A. Solbrand, H. Rensmo, J. Hjelm, A. Hagfeldt, S.-E. Lindquist, *J. Phys. Chem. B* **1997**, *101*, 7717.
- [38] P. P. R. M. L. Harks, C. B. Robledo, T. W. Verhallen, P. H. L. Notten, F. M. Mulder, *Adv. Energy Mater.* **2016**, *7*, 1601635.
- [39] S. S. Zhang, *Electrochem. Commun.* **2013**, *31*, 10.
- [40] H. J. Peng, J. Q. Huang, X. Y. Liu, X. B. Cheng, W. T. Xu, C. Z. Zhao, F. Wei, Q. Zhang, *J. Am. Chem. Soc.* **2017**, *139*, 8458.
- [41] J.-W. Park, K. Yamauchi, E. Takashima, N. Tachikawa, K. Ueno, K. Dokko, M. Watanabe, *J. Phys. Chem. C* **2013**, *117*, 4431.
- [42] D. Aurbach, G. S. Suresh, E. Levi, A. Mitelman, O. Mizrahi, O. Chusid, M. Brunelli, *Adv. Mater.* **2007**, *19*, 4260.